# EFFECT OF DYNAMIC COUPLING ON THE PERFORMANCE OF PISTON PUMP LUBRICATING INTERFACES

**SWARNAVA MUKHERJEE[1], SHANMUKH SARODE[1], CHINMAYEE MUJUMDAR[1], LIZHI SHANG[2], ANDREA VACCA[2]**

[1] School of Mechanical Engineering, Purdue University, West Lafayette, Indiana, USA

[2] School of Mechanical Engineering and Department of Agricultural and Biological Engineering, Purdue University, West Lafayette, Indiana, USA

**DOI: 10.17973/MMSJ.2022_10_2022075**

**mukher25@purdue.edu**

The energy efficiency and durability performance of axial piston machines are strongly affected by the tribological behavior of their lubricating interfaces. State-of-the-art approaches typically study these interface in isolation, neglecting possible reciprocal interactions between such interfaces. This paper presents an investigation of the mutual interaction between the piston/cylinder interface and the slipper/swashplate interface of a commercial axial piston pump. The proposed model can predict distributive fluid behavior in the lubricating gaps considering the effects of dynamics of the solid bodies, compressibility, mixed lubrication, elastic deformation, and cavitation. The dynamic coupling between the piston and the slipper is achieved by modeling the friction between the piston ball and slipper socket based on the force balance and the relative motion between the two bodies. The efficiencies predicted by this coupled model are compared to the ones obtained through the more established approach of solving the lubricating interfaces independently. The simulation results demonstrate the influence of the coupled physics on the lubricating interface performance, confirming the necessity of considering couple dynamics in lubricating interface numerical modeling.

**KEYWORDS**

Swashplate type axial piston machine, Lubricating interface, Piston/Cylinder interface, Slipper/swashplate interface, Modeling, Simulation, Coupled dynamics

## 1 INTRODUCTION

Axial piston machines (APMs) are widely used in fluid power applications, fuel injection and fluid transport systems owing to their superior power density, efficiency, and high-pressure capability. The performance of a swashplate type APM is dominated by the three main lubricating interfaces: the piston/cylinder interface, slipper/swashplate interface, and the cylinder block/valve plate interface. Therefore, in the past few decades significant efforts has been put in accurately model the performance of the lubricating interfaces.

Wieczorek and Ivantysynova[1] introduced a numerical simulation tool CASPAR to study the individual lubricating interfaces of an APM, considering the micromotion of rigid bodies and simplified fluid properties. A similar approach was extended to study the fluid-structure and thermal interactions in the piston/cylinder interface by Pelosi and Ivantysynova[2]. Further thermodynamic considerations were incorporated for the piston/cylinder interface by Shang[3]. A fluid-structure and thermal interaction model for the slipper/swashplate interface was introduced by Schenk and Ivantysynova[4]. A similar model for the cylinder block/valve plate interface was introduced by Zecchi[5],[6]. Relevant works outside the author's research group include one by Hashemi et al[7], presenting the use of Tribo-X, which includes the effects of mixed lubrication and fluid cavitation to analyze the slipper-swashplate interface. Gels and Murrenhoff[8] published a piston-cylinder interface numerical model for contoured profiles. They also reported the experimental validation of their model. Bergada et al[9],[10] studied the lubricating films between the cylinder block and valve plate as well as the slipper and swashplate.

However, one important shortcoming of the above-mentioned works is that the mutual interaction between the gap forces is not considered or is highly simplified. For example, the frictional moments in the piston/slipper ball joint are ignored in Pelosi[11] and Schenk's[4] work when calculating the tilting motion of the piston or the slipper body. However, the same frictional moments are assumed infinite when predefining the piston and slipper spinning speed as the same as the shaft speed. Moreover, the slipper spinning speeds were measured by Chao et al[12] and were found to be lower than the shaft speed. From the simulation studies in the same work, this slipper spin also has an impact on the tilting motion of the slipper body and changes the hydrodynamic pressure built in the slipper/swashplate interface. Recently, Zhao et al[13] validated the effect of piston spin inside the cylinder bore with the results predicted by Shirakashi et al[14] on the fluid film characteristics of a standalone piston/cylinder interface. The change in fluid film pressures and fluid film thickness will have a direct effect on the performance of the interface as well. However, the above models prescribed the amount of piston spin with respect to the shaft speed for different operating conditions studied. Although the studies successfully establish the effect of piston spin, the extent of piston spin is not predictable. Moreover, the piston/cylinder interface is directly connected to the slipper/swashplate interface with the ball joint, studying the effect of piston spin is more accurate when the lubricating interfaces are not isolated.

In the authors' research group as well, Ransegnola et al[15] developed a model to predict the relative spin between the piston and the slipper bodies by modeling friction in the ball socket joint friction and using the socket to communicate the moment balance between the piston/cylinder and slipper/swashplate interface. They concluded that the piston spin is heavily dependent on the friction in the ball socket joint and is a critical factor in the hydrodynamic pressure built in the piston/cylinder lubricating interface. However, the limitation of Ransegnola's work[15], is the lack of direct comparison between coupled and standalone simulation approaches.

The aim of this paper is to numerically quantify the effect of the dynamic coupling of the piston and slipper bodies in the piston/cylinder interface and slipper/swashplate interface performance by applying different assumptions of piston/slipper ball joint friction. The model used in this work is further developed from Ransegnola's model[15] to make the ball joint coupling effect configurable. Three configurations are studied in this paper. First, a dynamically coupled model that considers the friction forces in the ball socket joint based on a Stribeck friction curve is used to represent the most realistic assumption. The second configuration assumes that the piston and the slipper bodies are welded together. Therefore, the piston and the slipper bodies are rigidly connected. The third configuration decouples the two interfaces by applying no ball socket friction, essentially eliminating any mutual interaction between the two bodies. The paper also compares the leakage and shear effects

in both interfaces at different ball joint configurations. The authors also highlight the validity of each of the assumptions with respect to the operating conditions.

The current work first presents the approach taken to model each of the physical aspects involved in modeling of the system. The three different configurations of the ball socket joint are explained as well. Further, comparison between each of the ball socket configurations, for three different operating conditions on a reference unit, is made. The conditions that require an accurate modeling of the ball socket joint are discussed as well. Finally, conclusions are drawn based on the simulation study performed.

## 2 MODELING APPROACH

A multi-physics simulation suite, Multics CASPAR[16], developed at the authors' research center, was used to model a commercial swashplate type axial piston machine. The model comprises several sub-models as shown in Figure 1. The pressures in the displacement chambers, evaluated through a lumped parameter approach, are used to evaluate their resulting loads on the piston and slipper bodies. The piston and slipper dynamics modules solve for the 6 degrees of freedom equations of motion for each of these bodies. The resulting positions and velocities are then used to evaluate the squeeze and wedge effect on each of the three different lubricating interfaces. It is noted that the dynamics of the piston and slipper are coupled by utilizing a model for the ball socket joint between them. A brief description of each of the sub-models is provided in the current section.

### 2.1 Displacement chamber model

The displacement chamber model solves the isothermal pressure build-up equation in the displacement chambers and the slipper pockets. The pressure build-up equation is shown in Eq 1. The volume and volume derivative in Eq 1 is evaluated using the kinematic equation of the unit. $\dot{m}_{in}$ represents the net mass flux into a given displacement chamber or pocket at a given instance.

$$\frac{\partial p}{\partial t} = \frac{K}{V}\left(\frac{1}{\rho}\dot{m}_{in} - \frac{\partial V}{\partial t}\right) \tag{1}$$

The pockets are assumed to be connected to their respective displacement chambers through constant orifices and the net mass flux into them is evaluated using an orifice equation as shown in Eq 2.

$$\dot{m}_{in} = C_d A\sqrt{2\rho\Delta p} \tag{2}$$

The displacement chambers are assumed to be connected to the inlet and outlet ports with orifices of varying areas. These orifice areas represent the instantaneous flow restriction from a given displacement chamber to the outlet and inlet ports. To evaluate these areas, AVAS, a tool developed by Huang et al[14] is utilized. AVAS evaluates the minimum instantaneous cross-sectional area along the flow path from the displacement chamber to either of the ports by utilizing 3D drawings of the unit. It solves for an inviscid flow equation along the flow path and consecutively tracks the perpendicular cross-sectional area along the inviscid streamlines to store the minimum cross-sectional area. This evaluation is performed at incremental shaft angles to store the mentioned orifice area variation over a complete shaft rotation.

The displacement chamber and slipper pocket pressures evaluated using the lumped parameter approach is used to provide boundary conditions to the lubricating interface model as well as to evaluate the loads applied on the piston and slipper.

### 2.2 Lubricating interface model

The three main lubricating interfaces of a swashplate type axial piston machine are the slipper/swashplate interface, the piston/cylinder interface, and the cylinder block/valve plate interface. For the scope of this study, the analysis is restricted to the piston/cylinder and slipper/swashplate interfaces. The governing equation that dictates the behavior of these lubricating interfaces, is the universal Reynolds equation shown in Eq 3.

$$\nabla\cdot\left(\phi_p\left(\frac{Kh^3}{12\mu}\nabla\rho\right)\right) = \nabla\cdot\left(\rho v\left(\phi_R R_q + \phi_C h\right)\right) + \nabla\cdot\left(\rho\frac{\phi_S}{2}R_q(v_t - v_b)\right) + \frac{\partial\rho\left(\phi_R R_q + \phi_C h\right)}{\partial t} \tag{3}$$

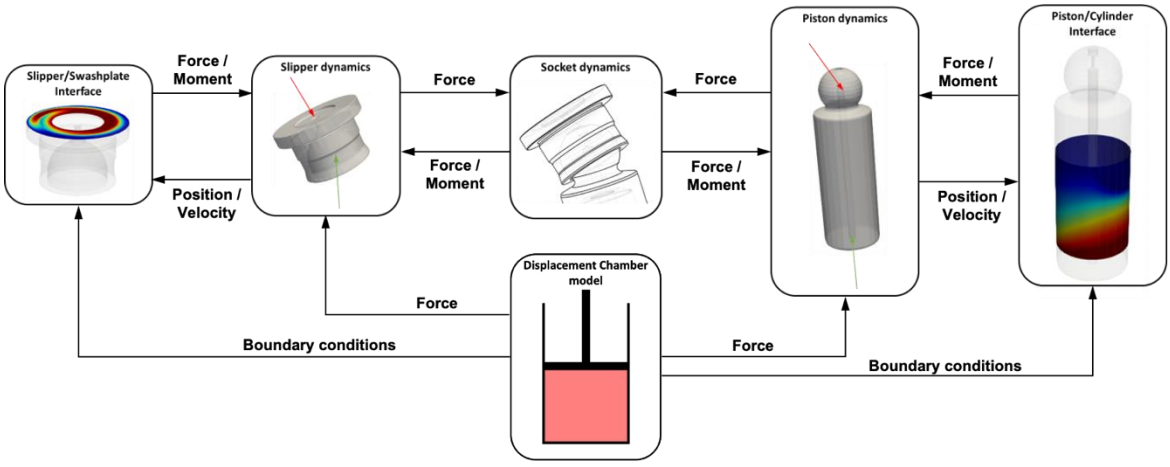


**Figure 1.** Model overview

It is observed that the Reynolds equation shown in Eq 3 is in terms of density. This form of the compressible Reynolds equation was derived by Ransegnola et al[16] and accounts for compressibility as well as cavitation in the lubricating interfaces. The formulation further incorporates the effects of mixed lubrication using stochastic flow factors: $\phi_p$, $\phi_R$, $\phi_S$ and $\phi_C$ as

shown by Patir and Cheng[17], [18]. The lubricating interface model also accounts for elastohydrodynamic effects by capturing the elastic deformation of the swashplate, slipper, piston and cylinder block using an influence matrix approach. The lubricating interface models provide the pressure and shear loadings to the corresponding bodies while using the positions and velocities of the same to dictate the squeeze and wedge effects.

### 2.3 Body dynamics

The body dynamics model solves for the conservation of linear and angular momentum on the slipper and piston.

An isolated free body diagram of the slipper is shown in Figure 2. $F_{BG,G}$ represents the load transferred to the slipper through the ball joint, as a result of the loads acting on the piston; $F_{HD}$ represents the force on the slipper as a result of the slipper hold down plate pressing against it; $F_{PG}$ represents the force on the slipper due to the hydrostatic pressure in the slipper pocket and$F_{FG}$ represents the pressure as well as shear forces on the slipper due to the hydrodynamic pressure build-up in the slipper/swashplate lubricating interface. It is noted here that$F_{PG}$ is evaluated using the slipper pocket pressure evaluated in the displacement chamber model and$F_{FG}$ is evaluated by integrating the pressure and shear stresses over the slipper land area, obtained using the lubricating interface model.

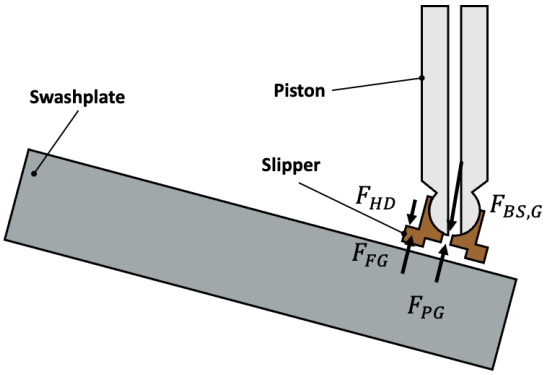


**Figure 2.** Slipper free body diagram

An isolated free body diagram of the piston is shown in Figure 3. $F_{DC}$ represents the axial force on the piston due to the pressurized fluid in the displacement chamber; $F_{BS,K}$ is the load transferred to the piston through the ball joint, as a result of the loads acting on the slipper. $F_{FK}$ represents the pressure and shear forces on the piston due to the hydrodynamic pressure build-up in the piston/cylinder lubricating interface. It is noted here that $F_{DC}$ is evaluated using the displacement chamber pressures obtained through the displacement chamber model, while$F_{FK}$ is evaluated by integrating the pressure and shear stresses over the piston running surface, obtained using the lubricating interface model.

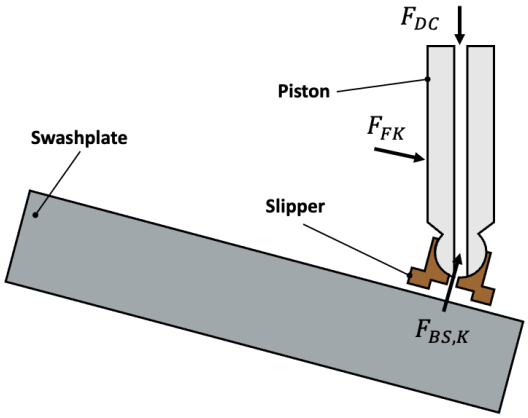


**Figure 3.** Piston free body diagram

### 2.4 Ball socket joint

The primary objective of the current work is to understand the effect of the coupling between the slipper and the piston. This coupling is established through the ball socket joint. To evaluate the load transfer between the piston and slipper, an important assumption pertaining to the ball socket joint is made. The clearance in the ball socket joint is assumed to be small enough that there exists no relative linear motion between the socket center of the slipper and the ball center of the piston. This assumption ensures that the linear accelerations of the piston and slipper remain the same. This can be expressed as shown in Eq 4, where $F_{net,K}$ represents the net force on the piston, $F_{net,G}$ represents the net force on the slipper, $m_K$ represents the mass of the piston and, $m_G$ represents the mass of the slipper. It is noted here that $F_{BS,K}$ and, $F_{BS,G}$ are the same in magnitude while being opposite in direction. Thus, solving Eq 4 yields the force that is transferred to the piston and slipper from the ball socket.

$$\frac{F_{net,K} + F_{BS,K}}{m_K} = \frac{F_{net,G} + F_{BS,G}}{m_G} \tag{4}$$

It is important to note that although there isn't a relative linear motion between the piston ball center and the slipper socket center, there exists a possibility of relative angular motion. Figure 4 shows the forces in the ball socket joint where $r_S$ is the radius vector from the center of the socket to the point of contact on its spherical surface, $F_{f,K}$ is the friction force on the piston as a result of the relative angular motion between the slipper and the piston. It is noted here that since the contact in the ball socket joint is spherical in nature, the radius vector to the point of contact and, $F_{BS,K}$ must lie on the same line of action. The ball socket joint in an axial piston machine is typically flooded with the working fluid and hence a Stribeck friction model as discussed in Armstrong et al[18] is used to model the friction force, $F_{f,K}$ as shown in Eq 5. $v$ represents the relative linear velocity at the point of contact, between the piston and the slipper, $v_{st}$ represents the Stribeck velocity threshold, $v_c$ represents the Coulomb velocity threshold, $\mu_S$ and $\mu_D$ represent the coefficients of static and dynamic friction between the materials and $F_{BS,K}$ represents the load transfer from Eq 4. The moment caused due to this frictional force is then evaluated by taking a cross product of this force with the effective moment arm at which it acts. An opposite moment is then applied to the slipper.


**Figure 4.** Forces in the ball socket

$$F_{f,K} = -\frac{\nu\sqrt{2e}}{v_{st}} F_{BS,K}(\mu_S - \mu_d) e^{\frac{-|\nu^2|}{v_{st}^2}} - \frac{\nu \mu_d F_{BS,K}}{|\nu|} \tanh\frac{|\nu|}{\nu_c} \quad (5)$$

The friction coefficient, $\mu_S$ and $\mu_D$ were chosen to be 0.16 and 0.08 respectively, which was demonstrated to be a successful value, for a brass slipper and a steel piston, by Ransegnola et al[15].

### 2.5 Zero relative motion model

The case wherein there exists no relative motion between the piston and the slipper, in other words, the piston and slipper being "welded" to each other, is also considered in the current work. In order to model the welded contact between the piston and the slipper, similar to Eq 4, a moment balance needs to be performed to ensure that the angular accelerations of the piston and slipper remain equal to each other. This is expressed as shown in Eq 6 where, $M_{net,K}$ is the net moment on the piston, $M_{net,G}$ is the net moment on the slipper, $\frac{\partial \omega_K}{\partial M_K}$ and $\frac{\partial \omega_G}{\partial M_G}$ are essentially the inverse of the inertial tensors of the piston and the slipper, $M_{BS,K}$ is the moment transferred from the slipper to the piston through the ball socket joint and $M_{BS,G}$ is the vice-versa.

$$\frac{\partial \omega_K}{\partial M_K}\left(M_{net,K} + M_{BS,K}\right) = \frac{\partial \omega_G}{\partial M_G}\left(M_{net,G} + M_{BS,G}\right) \quad (6)$$

### 2.6 Decoupled model

To evaluate the effect of the coupling between the piston and slipper through the ball socket joint, baseline simulations were also performed without the consideration of the ball socket model. In this case, the relative motion of the piston and slipper is not considered and the external loads acting on the piston are directly applied to the slipper and vice versa.

## 3 RESULTS AND DISCUSSION

After an extensive simulation study across the three different models discussed in the previous section, the results for moderate speed, moderate displacement, and a range of pressurizations are discussed in this section. Table 1 shows the different operating conditions that were simulated. All the operating conditions were at a $50\%$ displacement and a non-dimensional speed, $\frac{\omega}{\omega_{max}}$ of 0.6. It is noted that for the study presented, a commercial swashplate type axial piston machine was chosen with a displacement of 130cc/rev, maximum operating speed of 3500 rpm, maximum operating pressure of 400 bar and a maximum swashplate angle of 18 degrees. It is also noted that the pressurizations discussed are a subset of the operating conditions that were studied and found to reflect the differences across the three assumptions prominently.

| ***Operating condition*** | ***1*** | ***2*** | ***3*** |
|---|---|---|---|
| $\frac{\Delta p}{\Delta p_{max}}$ | 0.5 | 0.75 | 1 |

**Table 1 Simulation cases**

This section shows comparisons for a single set of piston/cylinder and slipper/swashplate interface, to provide emphasis on the differences between the three variations of modeling the ball socket joint.

Figure 5 shows the moment on the piston about its axis due to the shear forces in the piston/cylinder interface to highlight the effect of the forces and moments transferred through the ball socket joint. It should be noted that the moment is normalized with the theoretical moment given by Eq 7 where $V_{th}$ is the kinematic displacement of the unit and $\Delta p$ represents the operating pressure. Another remark for all the following figures is that shaft angles from 0-180 degrees correspond to the high-pressure stroke and 180-360 degrees correspond to the low-pressure stroke. It is observed that the general trend of the shear moment is very close among all the three variations of the model.

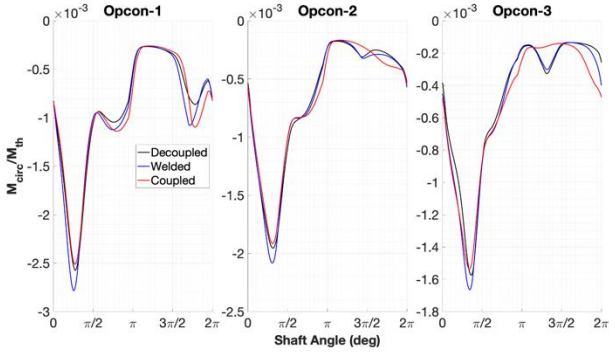


**Figure 5.** Shear moment on piston

$$M_{th} = V_{th}\Delta p \quad (7)$$

The non-dimensional axial forces on the piston, arising from the shear in the piston/cylinder interface are shown in Figure 8. It is noted here that the shear force is normalized with the average pressure force on the piston on the piston given by Eq 8 where $A_P$ is the projected area of the piston in the displacement chamber and $\Delta p$ is the operating pressure. It is observed that the axial shear forces show a similar conclusion as the shear moments wherein no significant difference between the different ball socket models is observed.

$$F_{\Delta p} = A_P \Delta \mathrm{p} \quad (8)$$

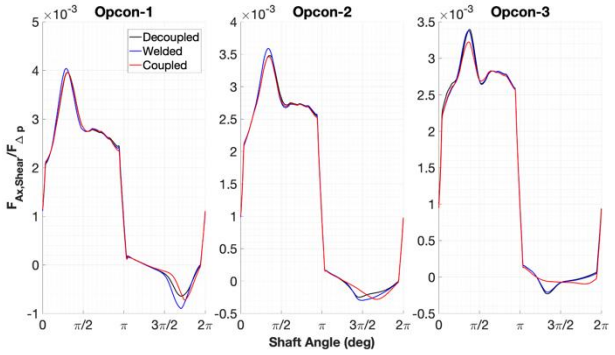


**Figure 6.** Axial shear on piston

A further look is provided at the piston/cylinder interface by the leakage flow from the displacement chamber to the case

through the interface shown in Figure 7. It is noted here that all the leakages are normalized with the kinematic flow rate of the unit given by Eq 9. The overall trend is observed to be very similar across all the different models of the ball socket joint.

$$Q_{th} = V_{th}\omega \tag{9}$$

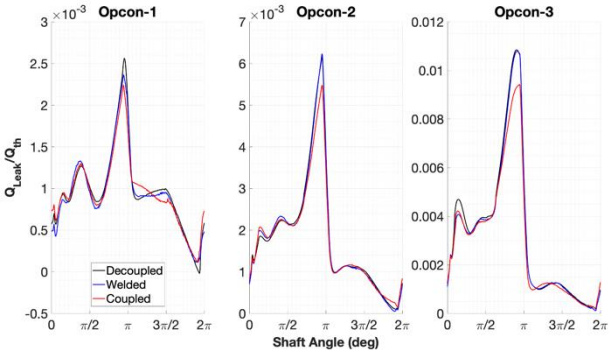


**Figure 7.** Piston film leakage

The normalized radial and tangential shear force on the slipper parallel to its running surface, which is directly responsible for the hydromechanical power loss, is shown in Figure 8 and Figure 9 respectively. One can observe how the decoupled and welded cases demonstrate a similar trend. The coupled case however demonstrates a larger difference in the shear forces. The difference is observed to be much higher, especially at higher pressure operating conditions. It is also observed that the difference among the ball socket models is more pronounced in the high-pressure strokes across all operating conditions.

The minimum non-dimensional film thickness occurring in the slipper/swashplate interface is shown in Figure 10. Here the film thickness is normalized with the nominal clearance of the interface. Examining Figure 10 with the non-dimensional maximum film thickness in the slipper/swashplate interface shown in Figure 11, reveals that the locations corresponding to a larger difference in the shear moments from Figure 8 also correspond to a larger amount of tilt in the slipper with the coupled model.

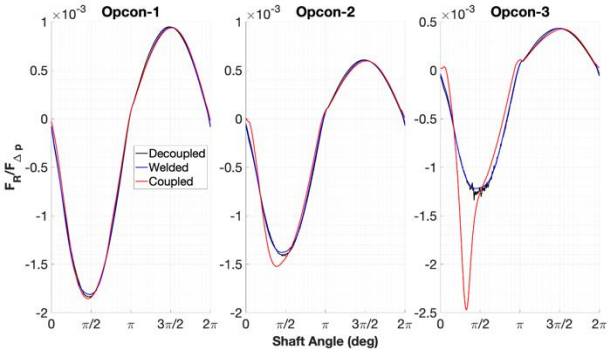


**Figure 8**. Radial shear force on slipper

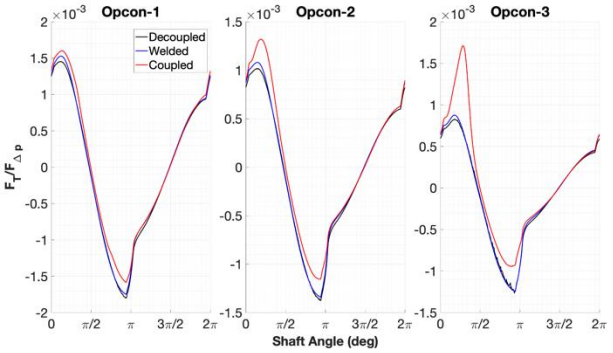


**Figure 9.** Tangential shear force on slipper

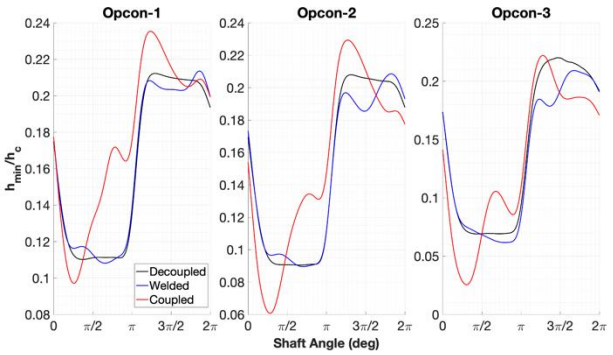


**Figure 10.** Slipper film minimum film thickness

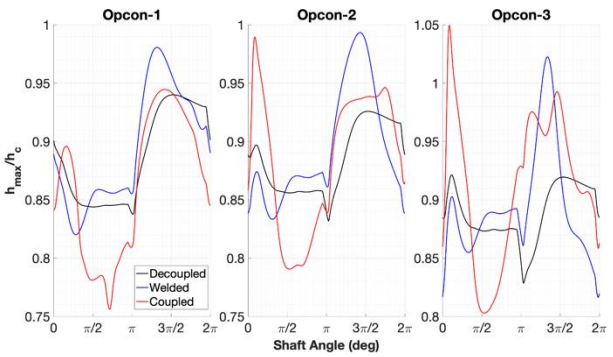


**Figure 11.** Slipper film maximum film thickness

To provide a wholesome representation of the slipper film thickness, plots of the slipper film thickness distribution for operating condition 3, for all the different variations of the ball socket model are shown in Figure 12. It is noted here that the unit under the current study uses a slipper with a recess on the land for better hydrodynamic support. The central ring-like structure in Figure 12 arises due to the mentioned recess. As with Figure 10 and Figure 11, Figure 12 also shows a high degree of similarity between the decoupled and welded models, although significant

differences are observed in the coupled model, especially at 30 and 90 degrees, which are a part of the high-pressure stroke.

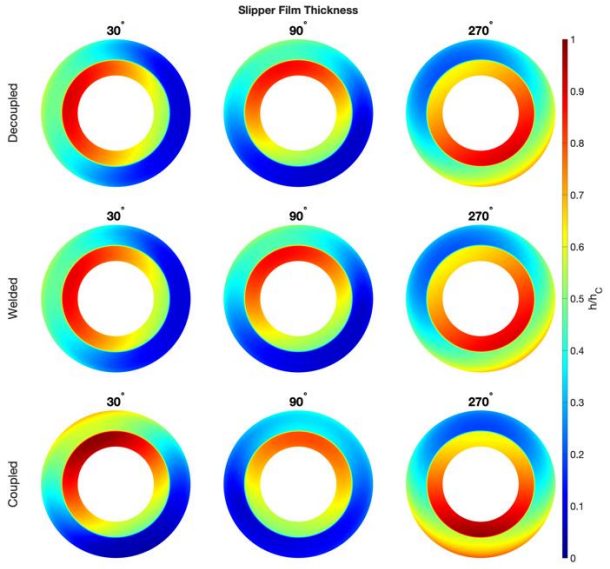


**Figure 12.** Slipper film thickness distribution

Figure 13 shows the normalized leakage from the slipper pocket to the case through the slipper/swashplate lubricating interface, which is directly responsible for the volumetric power loss. The differences between ball socket models show a similar trend as the shear moments from Figure 8.

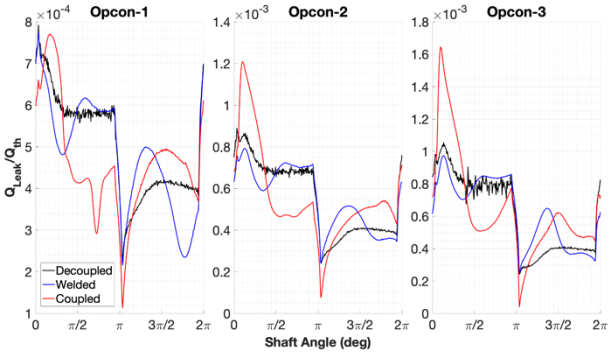


**Figure 13**. Slipper film leakage

The coupled model is observed to show trends in the slipper swashplate interface to be significantly different than the other two ball socket models. For a deeper insight into the slipper motion, Figure 14 is provided to illustrate the normalized tilt angle of the slipper about the swashplate displacement angle. It is observed that the welded model predicts a tilt angle that is slightly different from the decoupled model. But the coupled model predicts a much more severe tilt on the slipper, especially in the high-pressure stroke of all the operating conditions. The slipper is observed to switch its tilting on two different occasions in the high-pressure stroke. This switching is more apparent in the last two operating conditions. The first switch occurs at the beginning of the high-pressure stroke and the second switch occurs towards the end. The second switch can be attributed to the fact that the external loading on the slipper changes drastically from the high to the low-pressure stroke. The first switch on the other hand is caused due to the moments from the ball socket joint as shown in Figure 15. The general trend of the socket moment aligns with the displacement chamber pressures. Although, there exist certain peaks on the moment. These peaks correlate well with the switching in the slipper tilt angles from Figure 14.

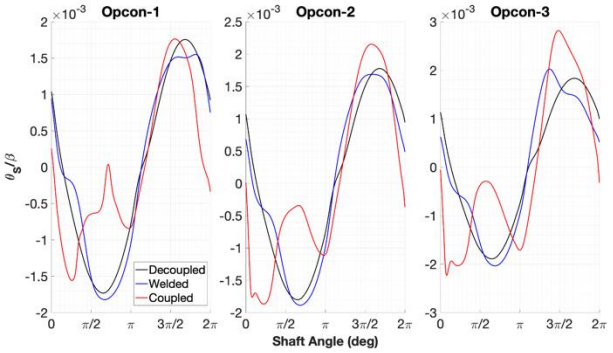


**Figure 14 Slipper tilt angle**

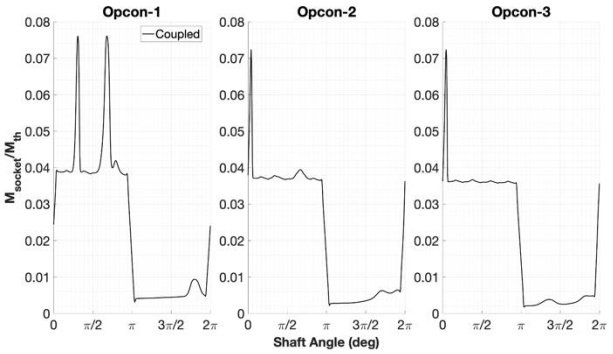


**Figure 15**. Socket moment

It can be inferred from the above discussion that the three different variations of the ball socket model predict the behavior of the piston/cylinder interface very closely. The differences arise during the high-pressure stroke for the slipper/swashplate interface. The differences arise due to the moments that the socket transfers to the slipper, from the piston. These differences are more pronounced in the high-pressure strokes and are minimal for the low-pressure stroke.

In order to further investigate the effect of the friction in the ball socket joint, a comparison of three different static friction coefficients (0.01, 0.16, and 0.18) is presented for the behavior of the slipper/swashplate interface.

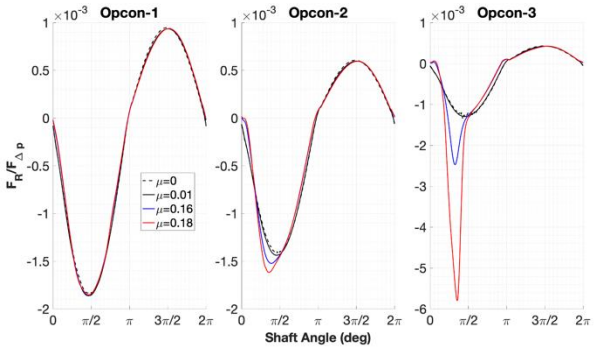


**Figure 16**. Effect of friction coefficient on radial shear force

Figure 16 and Figure 17 show the radial and tangential frictional forces on the slipper for the three different friction coefficients along with the decoupled or frictionless model for reference. As expected from the previous results, no significant differences are observed for the lower pressure operating condition. Although significant differences occur for the last two higher pressure operating conditions. It is worth noting that the results from the decoupled model are almost overlapping with those from the low friction coefficient which further increases confidence in the ball socket friction model. It is observed that the larger ball socket friction coefficient predicts a much higher frictional

resistance from the slipper/swashplate interface, especially through the high-pressure stroke.

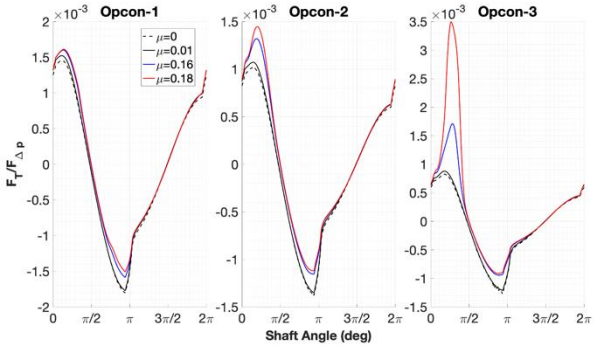


**Figure 17**. Effect of friction coefficient on tangential shear force

The effect of the ball socket friction on the volumetric leakage from the slipper pocket to the casing is shown in Figure 18. Although differences in leakage between the three friction coefficients are evident right from the low-pressure operating condition, significant differences are observed for the higher-pressure operating conditions. The higher the ball socket friction is, the larger the leakage during the high-pressure stroke. This trend is very similar to the shear losses in Figure 16 and Figure 17.

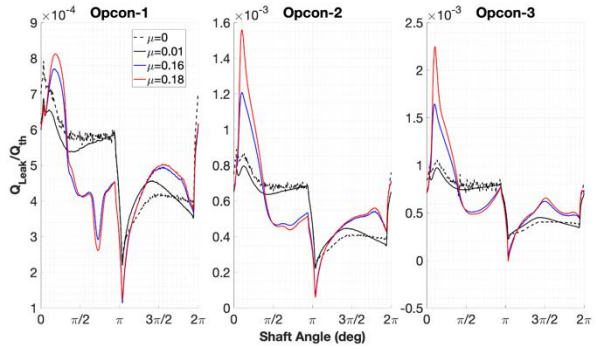


**Figure 18.** Effect of friction coefficient on slipper leakage

As discussed earlier in this section, the significant difference in the shear and leakage losses can be attributed to the slipper tilt originating due to the moments from the ball socket joint. The slipper tilt and the ball socket moments for the three different friction coefficients are shown in Figure 19 and Figure 20 respectively. It is observed here that the slipper tilt that is predicted with the ball socket model, is quite severe with the higher friction coefficients, especially at the higher-pressure operating conditions. A similar trend as the previous results, with the moments from the socket, is observed as well. Although, as expected, the magnitude of the moment is much higher for the higher friction coefficients.

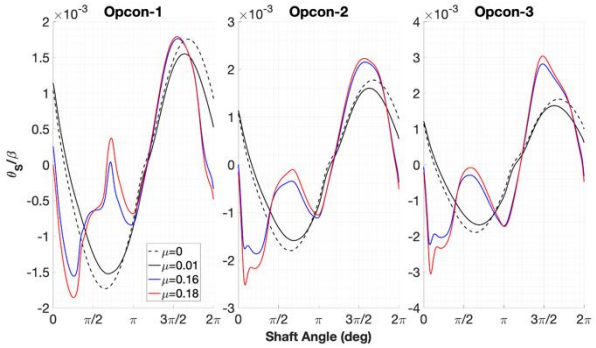


**Figure 19.** Effect of friction coefficient on slipper tilt

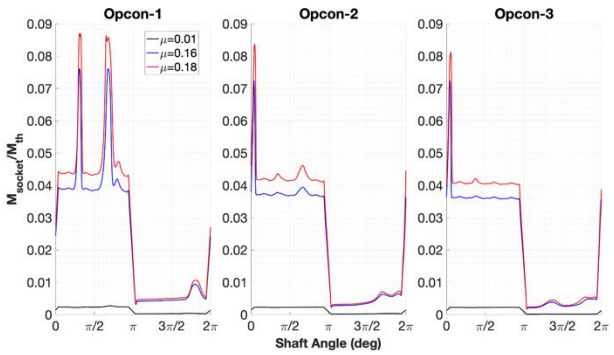


**Figure 20.** Effect of friction coefficient on socket moment

## 4 CONCLUSIONS

The recently developed Multics CASPAR model at the author's research center was utilized to study the mutual interaction between the piston/cylinder and slipper/swashplate interface of a swashplate type APM. The dynamics of the slipper and piston were coupled through a Stribeck friction-based model for the ball and socket joint. Three different variations of the ball socket joint between a piston and slipper were modeled: decoupled or frictionless, zero relative motion or welded, and coupled. The effects of these three models were studied on the piston/cylinder interface and the slipper/swashplate interface. Further, the effect of the friction coefficient of the ball socket joint was discussed. The results showed that the ball socket joint had a considerable effect on the shear and volumetric losses through slipper/swashplate interface while not having a significant effect on the piston/cylinder interface losses. Based on the discussions in the current study, it can be concluded that for applications involving design studies on the slipper, the considerations for the interaction between the piston/cylinder lubricating interface and the slipper/swashplate lubricating interface becomes a crucial component of the modeling approach. Additionally, the inclusion of such a model provides a more realistic estimation of the power losses from the unit, especially at higher pressure operating conditions. For example, the error in the net power loss from the slipper/swashplate interface for both the frictionless and welded assumptions in comparison to the coupled model for a ball friction coefficient of 0.18 was found to be about 30% for the highest-pressure operating condition. This is a significant difference when specifically designing the slipper/swashplate interface. It is however noted that this error also depends on the unit, operating condition and working fluid.

## 5 REFERENCES


[1] U. Wieczorek and M. Ivantysynova, "Computer Aided Optimization of Bearing and Sealing Gaps in Hydrostatic Machines—The Simulation Tool Caspar," *Int. J. Fluid Power*, vol. 3, no. 1, pp. 7–20, Jan. 2002.

[2] M. Pelosi and M. Ivantysynova, "Heat Transfer and Thermal Elastic Deformation Analysis on the Piston/Cylinder Interface of Axial Piston Machines," *J. Tribol.*, vol. 134, no. 4, Aug. 2012.

[3] L. Shang, "A Path Toward an Effective Scaling Approach for Axial Piston Machines," PhD Dissertation, Purdue University Graduate School, 2019.

[4] A. Schenk and M. Ivantysynova, "A Transient Thermoelastohydrodynamic Lubrication Model for the

Slipper/Swashplate in Axial Piston Machines," *J. Tribol.*, vol. 137, no. 3, Jul. 2015.

[5] M. Zecchi and M. Ivantysynova, "A novel approach to predict the cylinder block/valve plate interface performance in swash plate type axial piston machines," presented at the Bath/ASME Symposium on Fluid Power and Motion Control, Bath, UK, 2012.

[6] M. Zecchi, "A novel fluid structure interaction and thermal model to predict the cylinder block / valve plate interface performance in swash plate type axial piston machines," PhD Dissertation, Purdue University Graduate School, 2013.

[7] S. Hashemi, H. Friedrich, L. Bobach, and D. Bartel, "Validation of a thermal elastohydrodynamic multibody dynamics model of the slipper pad by friction force measurement in the axial piston pump," *Tribol. Int.*, vol. 115, pp. 319–337, Nov. 2017.

[8] S. Gels and H. Murrenhoff, "Simulation of the lubricating film between contoured piston and cylinder," *Int. J. Fluid Power*, vol. 11, no. 2, pp. 15–24, 2010.

[9] J. M. Bergada, D. L. Davies, S. Kumar, and J. Watton, "The effect of oil pressure and temperature on barrel film thickness and barrel dynamics of an axial piston pump," *Meccanica*, vol. 47, no. 3, pp. 639–654, Mar. 2012.

[10] J. M. Bergada, J. Watton, J. M. Haynes, and D. L. Davies, "The hydrostatic/hydrodynamic behavior of an axial piston pump slipper with multiple lands," *Meccanica*, vol. 45, no. 4, pp. 585–602, Aug. 2010.

[11] M. Pelosi and M. Ivantysynova, "A novel fluid-structure interaction model for lubricating gaps of piston machines," *WIT Trans. Built Environ.*, vol. 105, pp. 13–24, 2009.

[12] Q. Chao, J. Zhang, Q. Wang, B. Xu, and Y. Chen, "Experimental Verification of Slipper Spinning Motion in Axial Piston Pumps," ASME/BATH 2017 Symposium on Fluid Power and Motion Control, Oct. 2017.

[13] B. Zhao, X. Hu, H. Li, Y. Liu, B. Zhang, and Q. Dong, "A New Approach for Modeling Mixed Lubricated Piston-Cylinder Pairs of Variable Lengths in Swash-Plate Axial Piston Pumps," *Materials*, vol. 14, no. 19, p. 5836, Oct. 2021.

[14] Y. Fang and M. Shirakashi, "Mixed Lubrication Characteristics Between the Piston and Cylinder in Hydraulic Piston Pump-Motor," *J. Tribol.*, vol. 117, no. 1, pp. 80–85, Jan. 1995.

[15] T. Ransegnola, L. Shang, and A. Vacca, "A study of piston and slipper spin in swashplate type axial piston machines," *Tribol. Int.*, vol. 167, p. 107420, Mar. 2022.

[16] T. Ransegnola, "A Strongly Coupled Simulation Model of Positive Displacement Machines for Design and Optimization," PhD Dissertation, Purdue University Graduate School, 2020.

[17] N. Patir and H. S. Cheng, "Application of Average Flow Model to Lubrication Between Rough Sliding Surfaces," *J. Lubr. Technol.*, vol. 101, no. 2, pp. 220–220, Apr. 1979.

[18] N. Patir and H. S. Cheng, "An Average Flow Model for Determining Effects of Three-Dimensional Roughness on Partial Hydrodynamic Lubrication," *J. Lubr. Technol.*, vol. 100, no. 1, pp. 12–12, Jan. 1978.

**CONTACTS:**

Swarnava Mukherjee
Purdue University, School of Mechanical Engineering
1500 Kepner Dr., Lafayette, 47905, USA
+1(219)5762862, mukher25@purdue.edu,
https://engineering.purdue.edu/Maha/